Modeling Induced Master Motion in Force-Reflecting Teleoperation

Katherine J. Kuchenbecker and Günter Niemeyer

Stanford University Telerobotics Lab

http://telerobotics.stanford.edu

{*katherine.kuchenbecker, gunter.niemeyer*}*@stanford.edu*

Abstract— **Providing the user with high-fidelity force feedback has persistently challenged the field of telerobotics. Interaction forces measured at the remote site and displayed to the user cause unintended master device motion. This movement is interpreted as a command for the slave robot and can drive the closed-loop system unstable. This paper builds on a recently proposed approach for achieving stable, high-gain force reflection via cancellation of the master mechanism's induced motion. Such a strategy hinges on obtaining a good model of the master's response to force feedback. Herein, we present a thorough modeling approach based on successive isolation of system components, demonstrated on a one-degree-of-freedom testbed. A sixth-order mechanical model, including viscous and Coulomb friction as well as a new method for modeling hysteretic stiffness, describes the testbed's high-frequency resonant modes. This modeling method's ability to predict induced master motion should lead to significant improvements in force-reflecting teleoperation via the cancellation approach.**

Index Terms— **telerobotics, force feedback, haptic device, system identification, hysteresis modeling.**

I. INTRODUCTION

Teleoperation has long promised users the ability to perform manual tasks remotely, manipulating and perceiving an environment beyond normal human reach. The first such systems were developed in the late 1940s to allow an operator to handle radioactive materials from behind a shielded wall [1]. These master and slave robots were connected mechanically and acted as a single extended tool, allowing the user to feel all interaction forces directly through the mechanism. The flexibility of such systems was greatly increased by replacing the mechanical connection with an electric control system [2]. Unfortunately, providing natural force feedback has been a persistent challenge for this modern technology, even as it is used today for deep-sea exploration and minimally invasive surgery.

A perfectly transparent telerobotic system would portray the dynamics of the remote interaction without distorting the user's motions or haptic perceptions. Particularly important are the transient forces caused by contact between the remote manipulator and the environment [3]–[5]. These high-frequency vibrations convey important information about the material and geometry of the structures involved, increasing the realism of the interaction.
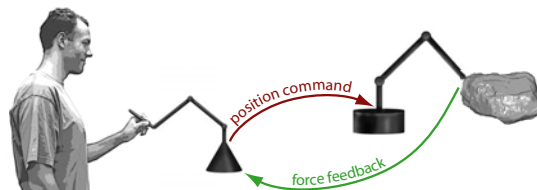

Fig. 1. Master and slave robots connect the user to the environment.

As illustrated in Fig. 1, many telerobotic controllers aim for transparency by commanding the slave to follow the measured position of the master. Forces sensed at the slave tip are simultaneously displayed to the user via the master's motors. The dynamics of the master couple its sensing and actuating functions together, inadvertently feeding the system's output back into its input. Like sound system speakers located too close to the microphone, high-frequency force feedback induces motion of the master device that is then interpreted as a position command. During environmental contact, this induced motion can cause unstable high-frequency vibrations, similar to the screeching of a badly configured sound system. As with speaker volume, force feedback must usually be attenuated to achieve stability, reducing haptic cues to the user and leaving interactions feeling soft and ill-defined.

We have proposed a new method for stably achieving high-gain force reflection by canceling this induced master motion from the slave command [6]. The linear second-order master model used in early work enabled a three-fold increase in the stable force-feedback gain of a one-degree-of-freedom (dof) testbed. This work seeks to develop a more detailed method for modeling master dynamics to allow even higher force reflection gains, heightened user sensitivity, and more robust stability.

This paper describes the modeling process required to create a successful cancellation controller. We begin by formally defining the cancellation approach in Sec. II and examining the dynamics of a typical master system in Sec. III. Section IV details the process of master identification, utilizing nonlinear friction and hysteresis elements and illustrating results on a one-dof testbed. We conclude our discussion in Sec. V by evaluating the presented methodology.
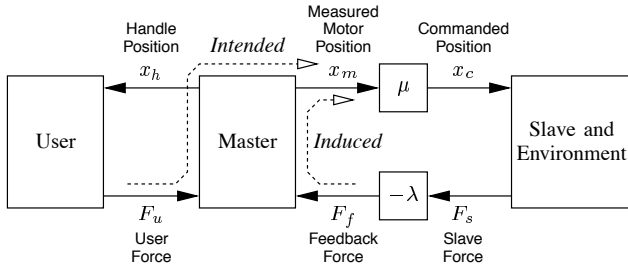
Fig. 2. Intended and induced motion of the master mechanism combine to form the slave command in position-force control.

Fig. 3. Induced master motion can be canceled using the model $\hat{G}_f$.

II. CANCELING INDUCED MASTER MOTION

Telerobotic systems often use position-force control to allow the user to feel the remote robot's contact with the environment. Using a force sensor hides inertial and frictional forces and captures the high-frequency transients that occur at contact. Such a controller is illustrated in Fig. 2, using μ as the forward position scale and λ as the force feedback gain. The master's two inputs of user force, applied at the handle, and feedback force, applied at the motor, together determine its measured motor position and thus the slave robot's commanded position. Movement caused by force feedback is not intended by the human but is rather an artifact of the master's dynamics. Along with the slave and the environment, the induced motion pathway closes an internal controller loop that is unstable under high gain product, $\mu\lambda$. Many researchers have suggested methods for avoiding this instability, such as added master damping, force feedback filtering, and position command filtering, which are detailed in [6].

As an alternative to the loop-shaping strategies proposed by others, the cancellation approach aims to break the internal loop of the controller. Assuming superposition, the dynamics of the master can be viewed as four input-output relationships from user force and feedback force to handle position and motor position, as illustrated in Fig. 3. We distinguish x_{mf} as deviations from the user's intended path caused by the feedback force, and we estimate it via the model $\hat{G}_f$. The model's response, $\hat{x}_{mf}$, is subtracted from the measured master position to provide an estimate of the user's intention, $\hat{x}_{mu}$, which is multiplied by μ to become the slave's position command. When the model closely approximates real system behavior, the direct connection from F_f to x_c will be attenuated, and the system will be stable for higher gain products $\mu\lambda$. The force feedback pathway to the user will not be affected, and the slave command will closely approximate user intention.

Achieving the theoretical benefits of cancellation requires an accurate model of master system dynamics. Daniel and McAree suggest viewing the relationship between force feedback and master motion in distinct power and information bands [7]. In the low-frequency power band, the mechanism moves as one entity, pushing against the user's hand during sustained remote contact. The structure of the master may deform slightly, but the user
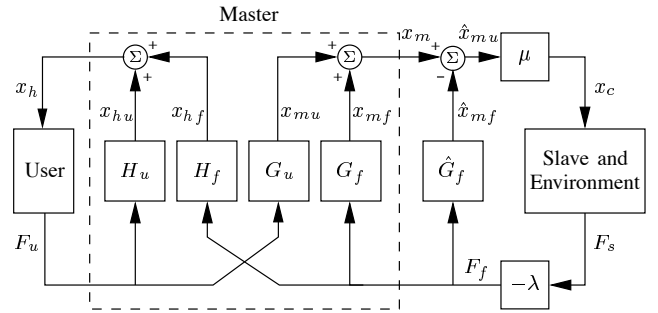
actively accounts for this deflection. In contrast, impacts create high-frequency transients that cause relative motion between the different components of the master. The user gleans important interaction information from these force signals but cannot actively control the high-frequency motion they induce. High gain-products $\mu\lambda$ destabilize telerobotic systems because force feedback transients directly affect the slave position command. A model that cancels this dynamic behavior will attenuate the controller's loop gain near crossover and stabilize the system.

III. MASTER MODEL

We can understand the behavior of the master mechanism under high-frequency force feedback by examining its components. Fig. 4 illustrates the chain of elements typically found in telerobotic masters. The controller runs on a real-time computer at a fixed servo rate, often one kilohertz. During each cycle, the feedback force is converted to a desired DC motor current and communicated to a self-contained linear or PWM amplifier. Motor current creates a torque on the motor shaft, and thin stranded cables couple the attached capstan to a larger drum, amplifying torque by a factor from ten to twenty. A mechanical linkage connects the drum to a handle, stylus, or thimble that the user holds. The entire mechanism is designed to be back-drivable with low inertia and low friction. Master motion is usually sensed with an optical encoder on the motor shaft, which provides a discrete position signal. Although differences exist, individual axes of most master mechanisms can be represented by such an arrangement.

Our early work approximated the master's most prominent high-frequency resonance as that of a linear mass-
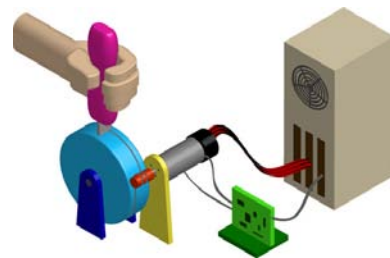

Fig. 4. The master's long dynamic chain connects the user and controller.
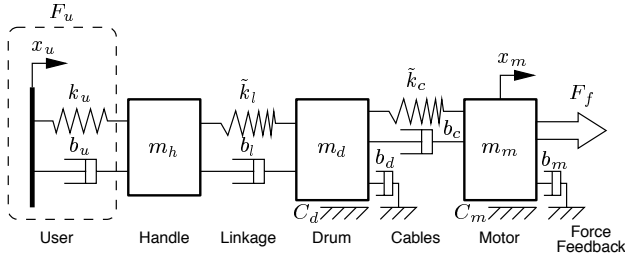
349

Fig. 5. Nonlinear lumped-parameter model of the master mechanism.

Fig. 6. One axis of an Impulse Engine 2000 is used as our master.

spring-damper [6], but such a simple model cannot capture the nonlinear and higher-order behavior of a real mechanism. A more accurate model may be obtained by separately identifying each of the system's dynamic elements. In particular, most master mechanisms can be approximated by the sixth-order model shown in Fig. 5. Rotation of the motor, drum, and handle are converted to equivalent translation of the user's hand, and inertial, stiffness, and dissipation parameters represent the effective values in this space.

The controller measures motor shaft motion, x_m, and commands the collocated feedback force, F_f. The motor shaft's rotational bearings are represented by both a Coulomb friction force, C_m, and viscous damping to ground, b_m. We define Coulomb friction as

$$C_m = \begin{cases} -c_m & \text{if } \dot{x}_m > 0 \\ 0 & \text{if } \dot{x}_m = 0 \\ +c_m & \text{if } \dot{x}_m < 0. \end{cases} \quad (1)$$

Commonly found at sliding interfaces, Coulomb friction causes linear rather than exponential transient decay.

The inertia of the motor, m_m, is linked to the inertia of the drum, m_d, via the cables. The cable stiffness, $\tilde{k}_c$, may be nonlinear, including hysteresis or position dependence, but the cable damping, b_c, can usually be described by linear viscosity. Like the motor, the drum model includes both a Coulomb friction force, C_d, and viscous damping to ground, b_d. A mechanical linkage with nonlinear stiffness, $\tilde{k}_l$, and viscous damping, b_l, connects the drum to the handle. The user force, F_u, is applied via an effective impedance, depicted as a linear spring and dashpot between the user's slowly changing desired position, x_u, and the mass of the handle, m_h. Many researchers use second-order models to describe passive biodynamics [8]–[10], and our previous investigations support the efficacy of such a user model in haptic interactions [6], [11]. Adding in the effects of servo loop timing, amplifier dynamics, and signal quantization, we now proceed to develop this sixth-order nonlinear mechanical model to capture the dynamic behavior of a master device during teleoperation.

IV. SYSTEM IDENTIFICATION

A detailed model of induced master motion, $\hat{G}_f$, can be developed through careful application of various identification techniques. The combined response of the master's many electronic and mechanical elements determines the relationship between commanded force feedback and measured motor position. Attempting to identify such a complex system all at once makes it hard to distinguish overlaid effects; instead we break the dynamic chain at points progressively farther away from the computer, applying force inputs such as sine waves and recording the resulting position response at each stage in the process. We demonstrate this strategy of successive isolation on our one-dof testbed, the Immersion Impulse Engine 2000 joystick shown in Fig. 6. Our investigations have characterized its forward/backward degree of freedom, keeping the left/right axis centered. The joystick is controlled via custom software on a personal computer running RTAI Linux. Building up an increasingly complex system model from the servo loop timing to the user's effective impedance, we change only the model's outermost parameters to match simulated to experimental behavior at each step.

A. Servo Loop Timing

A steady servo frequency is crucial for accurate system identification and model-based cancellation. Consistent timing can be verified by recording servo-cycle start times with the processor's timestamp clock or by observing triggered digital output lines with an oscilloscope. If timing variations are unavoidable, the controller can track time as it runs. Our RTAI platform achieves microsecond accuracy when executing a controller at five kilohertz.

B. Current Amplifier

The amplifier can add important dynamics to the haptic system and should be appropriately characterized. Particular attention should be paid to the following:

1) Steady-state gain, offset, linearity, and saturation.
2) Frequency response and high-frequency attenuation.
3) Maximum supply voltage and back-EMF effects.

For constant current commands, we used a high-precision ammeter to measure gain and offset and to verify linearity. Appropriate correction terms were incorporated into system software, and current saturation was included in our model. Spectral analysis was then used to verify the response of the testbed's linear amplifier up to one kilohertz. It performed almost ideally when the motor was stationary motor but could not reach maximum current at high motor speeds; we capture this effect by taking a real-time current measurement during all identification experiments.
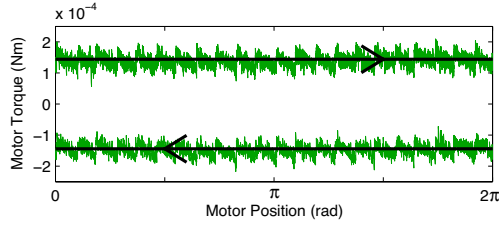
350

Fig. 7. Moving the motor under position control at various speeds reveals Coulomb friction and slight position dependence.

C. Motor and Encoder

The motor shaft, the first moving element in the master's dynamic chain, can be isolated by disconnecting the cables that couple it to the drum. The parameters of motor torque constant and encoder resolution may be measured or taken from appropriate data sheets. The local dissipation parameters of the motor, c_m and b_m, can then be identified using a closed-loop position controller. Recording the torque required to slowly rotate the motor in each direction provides a measure of its frictional losses. Performing this test at a range of speeds differentiates Coulomb friction, defined in (1), from velocity-dependent viscous friction. This test also illuminates any position-dependent friction, e.g. damaged motor bearings. The testbed's Maxon RE025-055-35 motor exhibits Coulomb friction only, varying insignificantly with commutator-brush position as illustrated in Fig. 7.

The motor shaft's total inertia can be estimated by summing the rotational inertias given on motor, encoder, and capstan data sheets. This value can be confirmed by observing the motor's step response under closed-loop position control, which acts as a virtual spring to ground and highlights the inertia via lightly damped oscillations. Starting with a model of the discrete servo cycle, the motor's identified friction, and the position controller, we fine-tuned the simulation's motor to match the system's observed time response. The parameters describing its viscous and Coulomb friction and combined inertia are transformed to tip space by ρ, the unitless motor to drum gear ratio, and h, the distance from the drum axis to the handle endpoint. The resulting values appear in Table I, which includes all identified model parameters.

TABLE I
IDENTIFIED MASTER MODEL PARAMETERS.

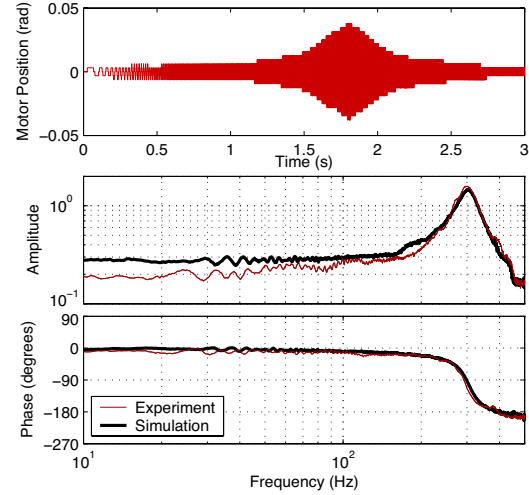| Parameter	Value	Parameter	Value
ρ	15 rad/rad	k_{lp}	3900 N/m
h	0.15 m	k_{ln}	4000 N/m
m_m	0.01075 kg	f_{lp}	0.465 N
b_m	0 Ns/m	f_{ln}	-0.445 N
c_m	.0144 N	γ_l	8500 rad/m
k_c	39500 N/m	b_l	0 Ns/m
b_c	3.6 Ns/m	m_h	0.014 kg
m_d	0.0075 kg	k_u	40 N/m
b_d	0.02 Ns/m	b_u	23 Ns/m
c_d	0.01 N		

Fig. 8. The cable/motor assembly exhibits a 300 Hz resonance that is well-matched in time and frequency domains by the nonlinear simulation.

D. Cables

The dynamic properties of the cables can be isolated by re-connecting them to the motor and locking the position of the drum. The cable should be tight enough to prevent relative motion between these two elements, but over-tightening increases the friction at this interface. Slowly varying motor torque across its full range and recording the resulting position waveform can usually provide only a rough stiffness estimate due to the small resulting motion. To augment this measurement, we applied a swept sine wave input that varied from 10 to 500 Hz to both the testbed and the simulation. Fig. 8 shows the actual motor's time response, clearly demonstrating a resonance, as well as an empirical transfer function estimate (ETFE) of both the experiment and the simulation after parameter fitting. The ETFEs can be viewed as experimentally determined Bode plots, showing the relationship between the frequency content of input and output signals. Even though our system is nonlinear, this technique can help us understand and model its resonant behavior. A simple spring and damper were found to adequately characterize the cables, and appropriate values were chosen for k_c and b_c.

E. Drum

The drum's inertial and frictional characteristics can be identified by disconnecting it from the linkage; on the joystick testbed, the linkage was separated where the bent member joins the beam from the base of the handle, splitting its small mass between the drum and the handle. The drum's parameters were identified by adding a position controller to the motor, grounding that end of the dynamic chain via a virtual spring. We then performed step responses of various magnitudes and with various controller position gains to elucidate the system's nonlinear behavior. A combination of hand-fitting and nonlinear
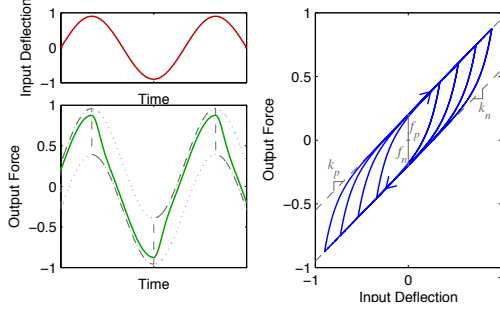
351

Fig. 9. A new hysteresis model was developed, switching between two stiffness asymptotes by velocity and spatially filtering the resulting force.
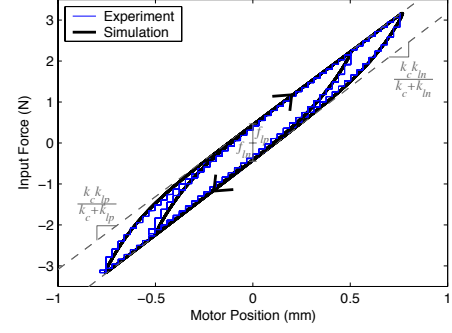

Fig. 10. The simulated linkage's force/position curve closely matches experimental observations.

Fig. 11. Adding hysteresis captures the linkage's nonlinear resonance.

unconstrained optimization were used to fit the parameters of m_d, b_d, and c_d, using a sum of squared position errors to quantify the accuracy of particular simulations. As with the motor, open-loop experiments that did not include a virtual grounding force were avoided; the unconstrained movements that result strongly depend on initial conditions and are not representative of the high-frequency oscillatory behavior that we wish to understand.

F. Linkage

After locking the handle position, the linkage can be examined using a force/position plot and a frequency response. The testbed's linkage was found to be an order of magnitude softer than the cables, and it displayed a rate-independent hysteresis, indicated by a significant enclosed area on its force/position plot. This hysteresis caused the system's resonant frequency and magnitude to depend strongly on input magnitude, a behavior that cannot be captured with a linear or position-dependent stiffness model. Unwilling to disregard this effect, we developed a new method for modeling hysteresis in dynamic systems.

Our model of hysteretic stiffness takes an input deflection and produces a smooth force signal, allowing it to be used in dynamic simulations. As shown in Fig. 9, repetitive deflections enclose an area in the force/position plot with a shape that matches that observed in actual elements. The model produces this output by switching between two offset stiffness lines based on positive or negative position changes and smoothing the output with a tunable spatial filter. The slope and vertical offset of the switching lines are denoted k_p and f_p for the positive motion asymptote and k_n and f_n for the negative motion asymptote. The coarse, pre-filtered force estimate is computed by

$$\hat{F}_i = \begin{cases} f_p + k_p x_i + k_p/\gamma & \text{if } x_i > x_{i-1} \\ \hat{F}_{i-1} & \text{if } x_i = x_{i-1} \\ f_n + k_n x_i - k_n/\gamma & \text{if } x_i < x_{i-1} \end{cases}, \quad (2)$$

where x is the deflection of the element, i is the index of the current servo cycle, and γ is the spatial filter bandwidth in radians per meter. We use a first-order filter to limit these discrete changes in force based on changes in position:

$$F_i = \frac{\gamma X}{1 + \gamma X}\hat{F}_i + \frac{1}{1 + \gamma X}F_{i-1}; \quad X = |x_i - x_{i-1}|. \quad (3)$$
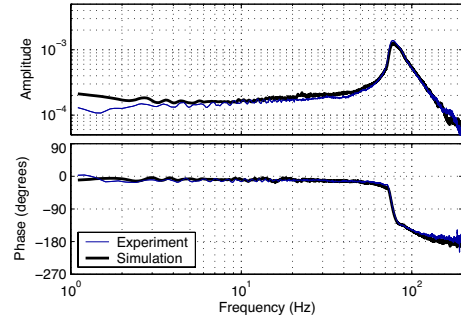
When the derivative of deflection is positive, the force gradually converges to $f_p + k_p x$, and when it is negative, the force converges to $f_n + k_n x$. The k/γ terms in (2) account for the steady-state error of the first-order filter. When the velocity changes sign and the raw force signal jumps to the other asymptote, the filter sees a combined step and ramp input, to which it has the constant steady state error k_{new}/γ. We correct for this effect by offsetting our asymptotes by the appropriate amount. To our knowledge, such a hysteresis model has not before been developed.

The new hysteresis model was added to the built-up simulation to represent the linkage stiffness. We slowly varied the testbed's feedback force and recorded the motor's resulting position change, as shown in the force/position plot of Fig. 10. The stiffnesses, k_{lp} and k_{ln}, were deduced from the experimental data's positive and negative velocity asymptotes, which represent the series stiffness of linkage and cables. After parameter fitting, this simple model of rate-independent hysteresis aptly characterized linkage behavior; such a model may also be applied to compliant elements found in other dynamic systems.

A good hysteresis model is important because apparent stiffness strongly depends on deflection magnitude. Small deflections give a relatively stiffer appearance, so the system's resonant frequency changes with signal amplitude. Swept sine wave inputs of different magnitudes were applied to both the actual and simulated testbeds, with a sample result shown in Fig. 11. The two ETFEs match well, responding similarly for a range of input magnitudes.
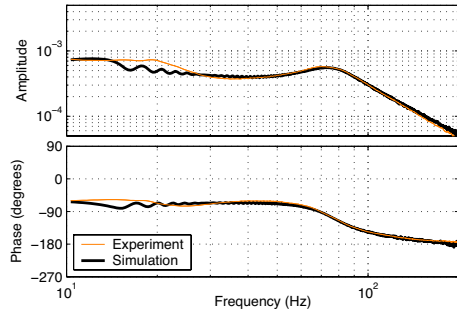
352

Fig. 12. The joystick resonates against the user's hand at 70 Hz.

Fig. 13. Two time responses verify the accuracy of the full system model.

This hysteresis model enables us to accurately characterize the master mechanism's response to high-frequency force feedback, as the shifting resonance cannot be adequately approximated with a linear model.

G. Handle and User Impedance

The last elements of the master's dynamic chain, the mass of the handle and the impedance of the user, can be characterized in the frequency domain. We applied swept sine waves from 10 to 200 Hz while a user held the joystick in a comfortable grasp. Fig. 12 shows the corresponding ETFE, to which the full model was matched via selection of m_h, k_u, and b_u. The subdued resonance at 70 Hz stems from the handle and mechanism vibrating against the flesh of the user's hand. This high-frequency induced master motion is rarely recognized but can destabilize a teleoperator.

H. Verification

To test the model's fidelity and thus its suitability for cancellation control, recorded impact forces were displayed on the master mechanism while held by a user. Two sample test results are shown in Fig. 13 as measured, estimated, and residual motor position traces. The model adeptly predicts system behavior for the first fifty milliseconds after impact before other effects such as the user's hand motion and reflexes alter the response. This detailed modeling method promises to be useful in the cancellation approach to telerobotic force feedback, where the difference between measured and simulated responses is used to form the slave motion command. Sudden master movement induced by force feedback is correctly estimated by the model and should be removed from the slave's position command.

V. CONCLUSION

Although often modeled as a simple mass, master mechanisms are comprised of several connected elements that all affect the system's dynamic behavior. This work presented a method for developing an accurate, high-order, nonlinear model of these dynamics for cancellation of induced master motion during force-reflecting teleoperation. Successive isolation of system components enables identification of Coulomb and viscous friction, inertia, nonlinear stiffness,
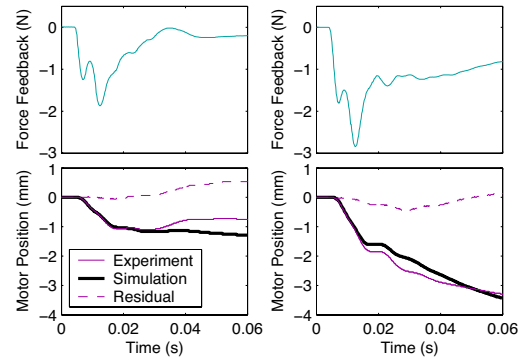
and user impedance. Additionally, we developed a new model for rate-independent hysteresis that matches behavior observed in the testbed's linkage, providing a smooth, hysteretic force signal suitable for dynamic simulations.

The complete joystick model, from motor to user impedance, was subjected to typical force signals and compared with experimental results; induced movement was predicted with approximately 90% accuracy. We anticipate that including this model in the cancellation approach will attenuate the induced motion pathway ten-fold, allowing for a ten-fold increase in stable force-feedback gain. The success of the developed model supports a promising future for the cancellation approach and the modeling methods presented herein.

REFERENCES

[1] R. C. Goertz, "Fundamentals of general-purpose remote manipulators," *Nucleonics*, vol. 10, no. 11, pp. 36–45, Nov. 1952.
[2] ——, "Electronically controlled manipulator," *Nucleonics*, vol. 12, no. 11, pp. 46–47, Nov. 1954.
[3] D. A. Kontarinis and R. D. Howe, "Tactile display of vibratory information in teleoperation and virtual environments," *Presence*, vol. 4, no. 4, pp. 387–402, 1995.
[4] A. M. Okamura, J. T. Dennerlein, and R. D. Howe, "Vibration feedback models for virtual environments," in *Proc. IEEE Int. Conf. Robotics and Automation*, May 1998, pp. 674–679.
[5] A. M. Okamura, M. Cutkosky, and J. T. Dennerlein, "Reality-based models for vibration feedback in virtual environments," *IEEE/ASME Trans. Mechatronics*, vol. 6, no. 3, pp. 245–252, Sept. 2001.
[6] K. J. Kuchenbecker and G. Niemeyer, "Canceling induced master motion in force-reflecting teleoperation," in *Proc. Int. Mechanical Engineering Conf. and Exposition*, Nov. 2004.
[7] R. W. Daniel and P. R. McAree, "Fundamental limits of performance for force reflecting teleoperation," *Int. J. Robotics Research*, vol. 17, no. 8, pp. 811–830, Aug. 1998.
[8] N. Hogan, "Controlling impedance at the man / machine interface," in *Proc. IEEE Int. Conf. Robotics and Automation*, vol. 3, May 1989, pp. 1626–1631.
[9] R. E. Kearney and I. W. Hunter, "System identification of human joint dynamics," *Critical Reviews in Biomedical Engineering*, vol. 18, no. 1, pp. 55–87, 1990.
[10] C. J. Hasser and M. R. Cutkosky, "System identification of the human grasping a haptic knob," in *Proc. Symp. Haptic Interfaces*, Mar. 2002, pp. 171–180.
[11] K. J. Kuchenbecker, J. G. Park, and G. Niemeyer, "Characterizing the human wrist for improved haptic interaction," in *Proc. Int. Mechanical Engineering Conf. and Exposition*, Nov. 2003.